

Table 3.4

Results of Weight Ratios with Respect to Sn
for the NBS Metal Alloy Standards

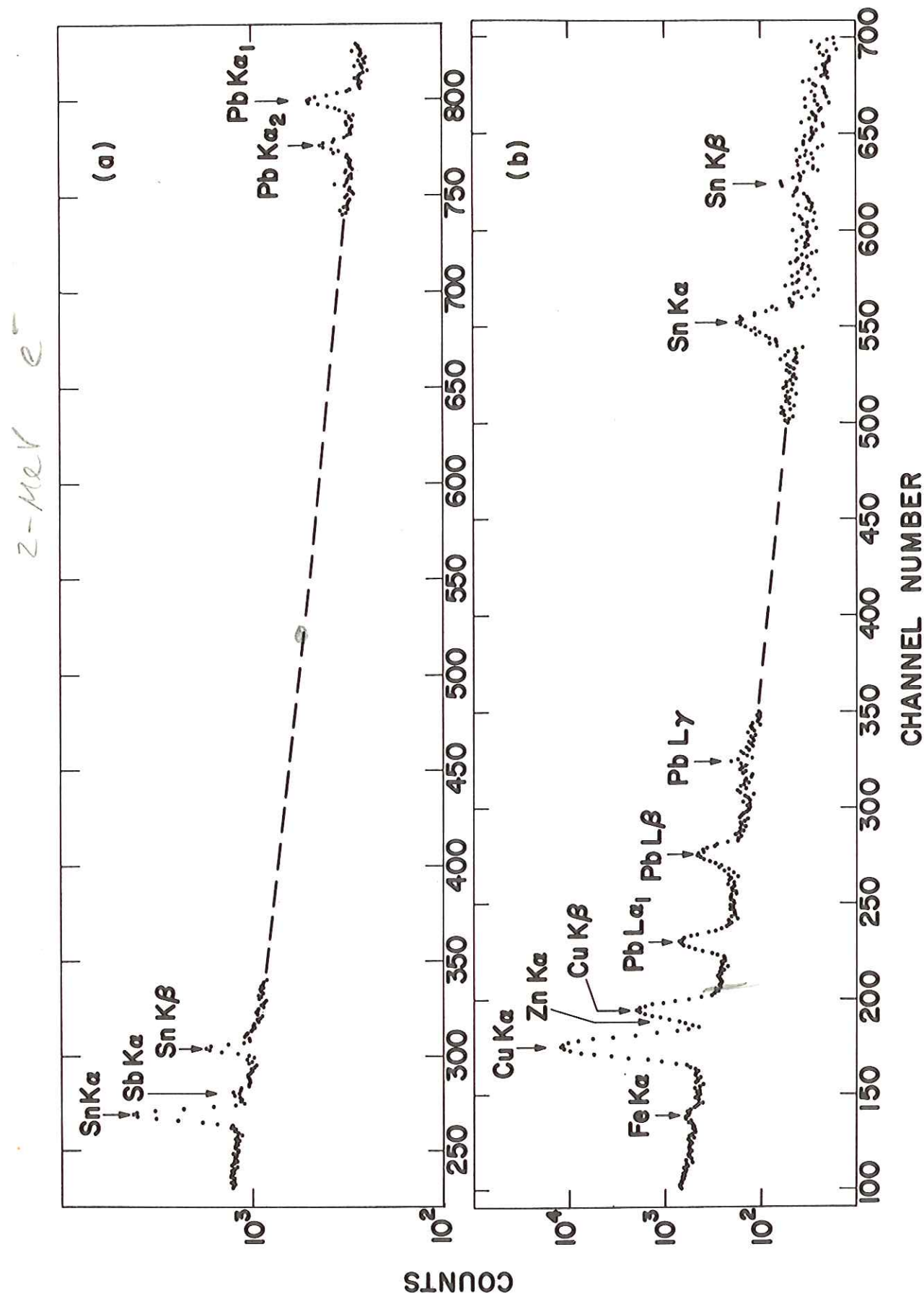
	$\frac{m_{Sb}}{m_{Sn}}$	$\frac{m_{Pb}}{m_{Sn}}$
<u>NBS-52</u>		
Reported*	0.0203	0.1924
Found Ge(Li)	-	0.1382
Found Si(Li)	-	0.2104
<u>NBS-54</u>		
Reported*	0.0831	0.0063
Found Ge(Li)	0.0835	-
Found Si(Li)	0.0823	0.0061
<u>NBS-63</u>		
Reported*	0.0555	0.9828
Found Ge(Li)	0.0592	1.058
Found Si(Li)	-	1.023

*Refer to Tables 2.4, 2.5 and 2.6.

FIGURE 3.5

X-Ray Spectra of the Phosphor Bronze
Bearing Metal (NBS No. 63)

- (a) Obtained with the Ge(Li) detector (System C) in a 58 minute run with 2 MeV electrons at 50 nA current.
- (b) Obtained with the Si(Li) detector (System D) in a 17 minute run with 2 MeV electrons at 85 nA current.



the Ge(Li) spectra had a small contamination of Pb X-ray background arising from the lead shielding in System D. Although small, this background accounted for 10% of the observed K α X-ray peak in the spectrum for NBS No. 63 and 50% of that for NBS No. 52. There is little difference between the results obtained with the Si(Li) and Ge(Li) detectors for the $m_{\text{Sb}}/m_{\text{Sn}}$ determination. This is due to the fact that the relative yields for the Sb K α and Sn K α are almost identical for both detectors.

Table 3.5 contains the results of assays for Sn, Zn, Pb, Sb and Fe with respect to Cu in the three NBS samples as measured from spectra obtained with the Si(Li) detector. A typical spectrum that for the cast bronze (NBS No. 52) is shown in Figure 3.6a. Except for the lead analysis which used the Pb L α_1 and L β lines, the K α X-rays of each element were used for the determinations. As shown in Table 3.5, all the weight ratios, except those for $m_{\text{Fe}}/m_{\text{Cu}}$, were determined with less than 15% differences from the NBS reported values. In the iron analyses, correction had to be made for the Cu produced Si X-ray escape peak (Cu K α - Si K = 6.3 keV) which underlies the Fe K α X-ray (6.4 keV). Although the escape peak loss for Cu K α X-rays was independently measured to less than 1% [$R = (6.27 \pm 0.31) \times 10^{-3}$], it is a significant correction when there is a small amount of Fe in the presence of a large amount of Cu as for the present cases. A discussion and description of this measurement of R is provided in Appendix A. Even with these large corrections, the $m_{\text{Fe}}/m_{\text{Cu}}$ weight ratios obtained were within 10-30% of the reported values. To determine the $m_{\text{Zn}}/m_{\text{Cu}}$ weight ratio, the Zn K α peak had to be stripped from the Cu K α and K β peaks using

Table 3.5

Results of Weight Ratios with Respect to Cu
for the NBS Metal Alloy Standards

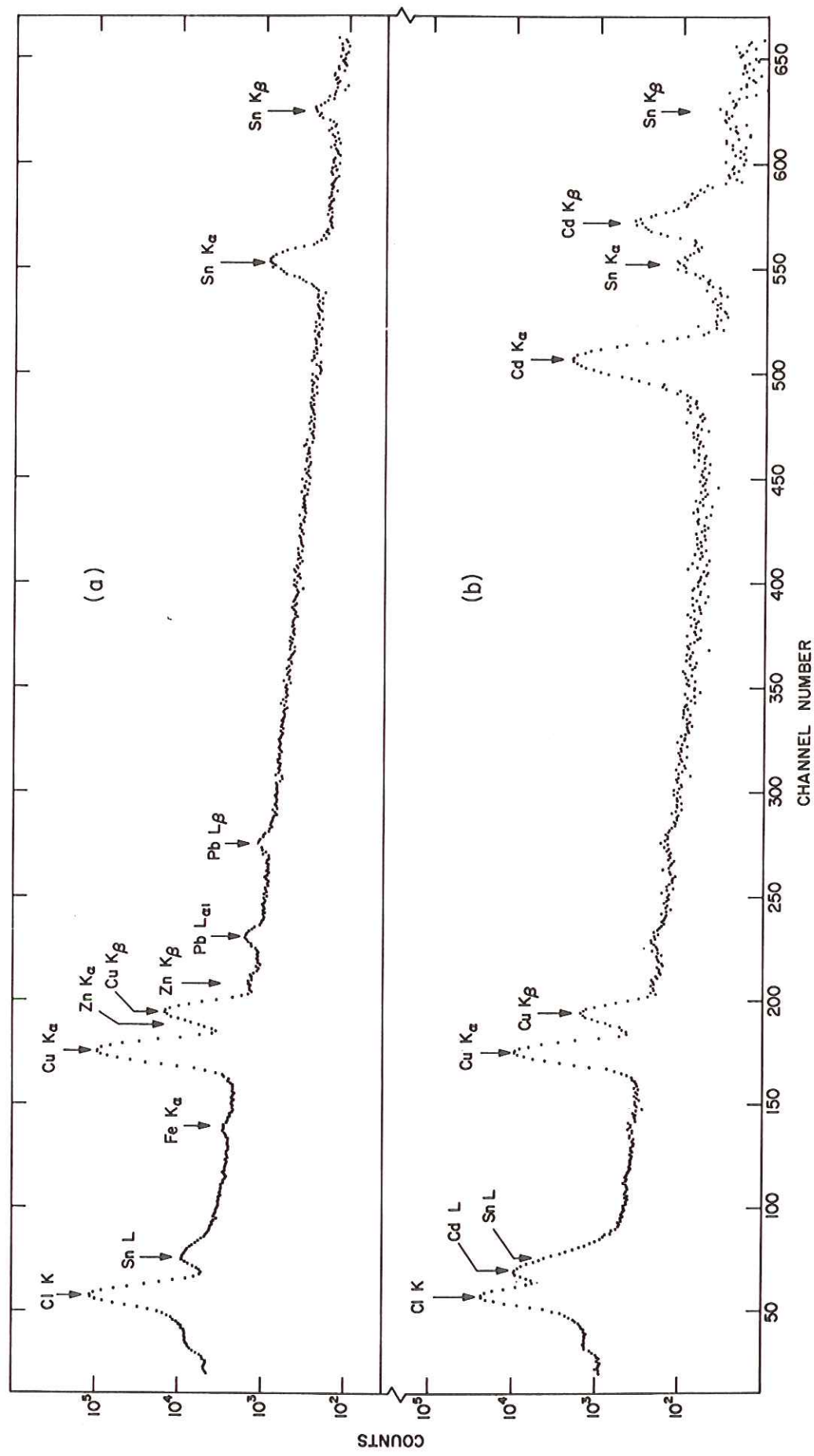
	<u>m_{Sn}/m_{Cu}</u>	<u>m_{Zn}/m_{Cu}</u>	<u>m_{Pb}/m_{Cu}</u>	<u>m_{Sb}/m_{Cu}</u>	<u>m_{Fe}/m_{Cu}</u>
<u>NBS-52</u>					
Reported*	0.0894	0.0214	0.0172	0.0018	0.0014
Found Si(Li)	0.0877	0.0183	0.0185	-	0.0018
<u>NBS-54</u>					
Reported*	25.53	-	0.1493	1.955	0.0160
Found Si(Li)	22.75	-	0.1390	1.871	0.0191
<u>NBS-63</u>					
Reported*	0.1270	0.00615	0.1248	0.00705	0.00346
Found Si(Li)	0.1197	0.00613	0.1224	-	0.00376

*Refer to Tables 2.4, 2.5 and 2.6.

FIGURE 3.6

X-Ray Spectra of the Cast Bronze (NBS No. 52)
Obtained with the Si(Li) Detector (System C)

- (a) in a 180 minute run with 2 MeV electrons at 30 nA current.
- (b) with reference Cd (weight ratio: 0.5613) in a 27 minute run with 2 MeV electrons at 25 nA current.



their standard line shapes obtained from the reference sample spectra. Although these Zn K α peaks were not clearly distinct in the spectra (see, for example, Figure 3.6a), the differences in m_{Zn}/m_{Cu} from the reported assays were - 14% (NBS No. 52) and less than + 1% (NBS No. 63) for the two samples containing zinc. Nickel which was present in two of the samples (NBS No. 52 and 63) was not detected since it was present in only small amounts and was masked by the intense Cu K α and Cu K β X-ray peaks. Similarly, antimony was not detected in two cases since it was present in low concentrations and was partially masked by the Sn K X-rays. For NBS No. 54 which has 7.33% Sb in the sample (see Table 2.5), it was detected and the m_{Sb}/m_{Cu} ratio was determined with a 4% difference from the NBS value. In comparison, the m_{Sb}/m_{Sn} weight ratio differed from the reported value by less than 1% (compare Tables 3.4 and 3.5). This illustrates the point that a given element may be determined much more accurately with respect to one element than to another. That is, it may be possible to determine a particular pair of elements very accurately, in this case Sn and Sb; whereas, the same element in another pair, viz. Cu and Sb, may not be determined as well. The Sb/Sn pair may be better in this case than the Sb/Cu pair because of the comparable absorption for the Sb and Sn K X-rays. At any rate, this can be important and advantageous when one is only interested in the relative amounts of two given elements in a sample. No effort was made to detect or determine the light elements ($Z < 20$). Because the samples were dissolved in acids containing chlorine, the Cl K X-rays masked this light element region (see Figure 3.5a). The L X-rays from heavier elements are also present in this region and as a result the

analysis becomes quite complicated.

The m_{Cu}/m_{total} weight ratios in the three NBS standards were determined from spectra of samples containing known weight ratios, m_{total}/m_{Cd} , of the standard to internal reference Cd weight. As an example, Figure 3.6b contains the spectrum for the cast bronze (NBS No. 52) sample. The weight ratios, m_{Cu}/m_{total} , were determined through the use of Equation 2.5 from the measured intensities of the Cu K α and Cd K α X-rays in the same spectrum and the known m_{total}/m_{Cd} weight ratio. The results in comparison to the NBS assays are provided in Table 3.6. For all three samples, the difference in the found and reported values was less than 7%. The results from the m_{Cu}/m_{total} (Table 3.6) and the m_Z/m_{Cu} (Table 3.5) weight ratios can be combined to obtain the percent of element Z in the sample. Thus, from the two sets of measurements, one can construct the percentage of each detected element in the total sample without detecting all of the sample's constituent elements. It must be emphasized that when this is done the errors on the two measurements compound, and of necessity, a weight ratio obtained from a single measurement is much more precise.

The elements determined in the three NBS standards ranged from 0.06% to 88%. In general, the determinations were in good approximate agreement with the reported assays. It should be recognized that the accuracy of these results is directly dependent on the statistics of the measured X-ray intensities which in turn is linearly dependent on the total time of the measurement. Longer runs would result in much better counting statistics and thus more precise and accurate measurements. The intent of these studies, however, was to demonstrate what

Table 3.6

Results of Weight Ratios with Respect to the Total Sample for the NBS Metal Alloy Standards

	$\frac{m_{Cu}}{m_{total}}$	$\frac{m_{Pb}}{m_{total}}$
<u>NBS-52</u>		
Reported*	0.8833	0.0152
Found Si(Li)	0.9178	-
<u>NBS-54</u>		
Reported*	0.0375	0.0056
Found Si(Li)	0.0377	-
<u>NBS-63</u>		
Reported*	0.7805	0.0974
Found Si(Li)	0.8321	0.0956

*Refer to Tables 2.4, 2.5 and 2.6.

could be done in relatively short periods of time. Although the matrix effects were compensated to first order (cf. Section 1.1.4) because of the similarity in the reference and unknown sample targets, no further matrix corrections were made to show what the developed method could do without these subtleties. One may anticipate a many fold increase in accuracy by increasing the counting time and making the presently available sophisticated corrections. At any rate, the present results are very encouraging. It was demonstrated that elemental analysis by energy dispersive X-ray spectroscopy following high energy electron impact ionization is suitable for rapid assays. The method can simultaneously determine a wide range of elements with comparable sensitivity, and it requires only a minimum of sample preparation. The determination for specific elements could also be markedly improved over the present results by the use of critical absorbers and other experimental considerations such as prior chemical separation.

3.2 Relative K-Shell Ionization Cross Sections

The relative $K\alpha$ X-ray yields, $Y_{K\alpha}(Z)$, can be used to obtain relative K-shell ionization cross sections, $\sigma_K(Z)/\sigma_K(Cd)$, as follows.

The detected number of $K\alpha$ X-rays from element Z produced by impact of $N_e(E)$ electrons with energy E on a target containing a_Z atoms per square centimeter is given by

$$N_{K\alpha}(Z) = a_Z N_e(E) \left[\frac{\sigma_K(Z, E) \omega_K(Z)}{1 + K\beta/K\alpha(Z)} \right] \epsilon_{K\alpha}(Z) \Omega T_{K\alpha}(Z) A_{K\alpha}(Z), \quad (3.1)$$

where $\sigma_K(Z, E)$ is the K-shell ionization cross section of element Z for electrons of energy E,
 $\omega_K(Z)$ is the K-shell fluorescence yield of element Z,
 $K\beta/K\alpha(Z)$ is the radiative transition probability ratio for $K\beta$ or $K\alpha$ X-rays of element Z,
 $\epsilon_{K\alpha}(Z)$ is the intrinsic detection efficiency for $K\alpha$ X-rays of element Z,
 Ω is the solid angle of the target subtended by the detector,
 $T_{K\alpha}(Z)$ is the fractional target transmission for $K\alpha$ X-rays of element Z produced in the target,
and $A_{K\alpha}(Z)$ is the correction for absorption of $K\alpha$ X-rays of element Z by materials interposed between the target and the detector.

Since the measured relative $K\alpha$ X-ray yields (see Equation 2.2) are given by

$$Y_{K\alpha}(Z) = \frac{N_{K\alpha}(Z)}{N_{K\alpha}(Cd)} \left(\frac{a_{Cd}}{a_Z} \right), \quad (3.2)$$

the K-shell ionization cross section for element Z at a given electron energy relative to that for Cd is

$$\frac{\sigma_K(Z, E)}{\sigma_K(Cd, E)} = Y_{K\alpha}(Z) \frac{\omega_K(Cd)}{\omega_K(Z)} \frac{[1 + K\beta/K\alpha(Z)]}{[1 + K\beta/K\alpha(Cd)]} \frac{\epsilon_{K\alpha}(Cd)}{\epsilon_{K\alpha}(Z)} \cdot \frac{T_{K\alpha}(Cd)}{T_{K\alpha}(Z)} \frac{A_{K\alpha}(Cd)}{A_{K\alpha}(Z)}. \quad (3.3)$$

In this way, the number of electrons, $N_e(E)$, incident on the target and the target solid angle do not have to be determined. Furthermore, none of the remaining terms of Equation 3.3 has to be absolutely known. Only the ratios of the values for element Z to that for Cd are necessary.

This is especially advantageous since the ratio of some of these terms, e.g., $\epsilon_{K\alpha}(Z)/\epsilon_{K\alpha}(Cd)$, may be determined very precisely; whereas, the absolute value of the individual terms are extremely difficult to measure.

The relative cross sections were determined from the relative yield data for System C and D which employed the lens tissue targets. The yields, $Y_{K\alpha}(Z)$, for the two systems are listed in Tables 3.2 and 3.3, respectively. As discussed in Section 3.1, the error limits on these relative yields are estimated to be $\pm 5\%$. Although these error limits could not be estimated formally since they were arrived at from value judgements and precision data, they are estimated to be larger than a 95/100 error. The values of the ratios $\omega_K(Z)/\omega_K(Cd)$, $[1 + K\beta/K\alpha(Z)]/[1 + K\beta/K\alpha(Cd)]$, $T_{K\alpha}(Z)/T_{K\alpha}(Cd)$, $A_{K\alpha}(Z)/A_{K\alpha}(Cd)$ and $\epsilon_{K\alpha}(Z)/\epsilon_{K\alpha}(Cd)$, and their estimated uncertainties, which were used to obtain the relative cross sections from the yield data, are tabulated in Tables 3.7 and 3.8.

The K-shell fluorescence yields used to obtain the $\omega_K(Z)/\omega_K(Cd)$ ratios were taken from the compilation of Bambynek, Crasemann, Fink, et. al. (BCF72). As described in Section 1.1.3, these semiempirical ω_K values were obtained from a best fit of Equation 1.13 to "most reliable" critically evaluated experimental results. The error limits on the ratios were propagated from the total uncertainties on the fitted values as reported by Bambynek, et. al. (BCF72). The total uncertainty takes into account both the uncertainties in the fitting constant (see Equation 1.13) and the uncertainties due to systematic errors in the

Table 3.7

Tabulation of Values for $\omega_K(Z)/\omega_K(\text{Cd})$, $[1 + K\beta/K\alpha(Z)]/[1 + K\beta/K\alpha(\text{Cd})]$,
 $T_{K\alpha}(Z)/T_{K\alpha}(\text{Cd})$ and $A_{K\alpha}(Z)/A_{K\alpha}(\text{Cd})$

Element	Z	$E_{K\alpha}(Z)$ (1) keV	$\omega_K(Z)$ (2)	$\frac{[1 + K\beta/K\alpha(Z)]}{[1 + K\beta/K\alpha(\text{Cd})]}$ (3)	$\frac{T_{K\alpha}(Z)}{T_{K\alpha}(\text{Cd})}$ (4)	$\frac{A_{K\alpha}(Z)}{A_{K\alpha}(\text{Cd})}$ (5)	$Ge(\text{Li})$ (a)	$Si(\text{Li})$ (b)
V	23	4.95	0.298 ± 0.013	0.908 ± 0.004	0.808 ± 0.019	-	0.982	-
Cr	24	5.41	0.336 ± 0.014	0.916 ± 0.004	0.829 ± 0.019	-	0.986	-
Mn	25	5.90	0.374 ± 0.030	0.922 ± 0.004	0.850 ± 0.020	-	0.988	-
Fe	26	6.40	0.413 ± 0.017	0.928 ± 0.004	0.870 ± 0.020	-	0.990	-
Co	27	6.93	0.454 ± 0.036	0.930 ± 0.004	0.889 ± 0.020	-	0.992	-
Ni	28	7.47	0.493 ± 0.037	0.932 ± 0.004	0.906 ± 0.021	-	0.994	-
Cu	29	8.04	0.530 ± 0.021	0.933 ± 0.004	0.919 ± 0.021	-	0.995	-
Zn	30	8.63	0.570 ± 0.041	0.935 ± 0.004	0.932 ± 0.021	-	0.997	-
As	33	10.53	0.675 ± 0.044	0.944 ± 0.004	0.961 ± 0.022	-	0.999	-
Se	34	11.21	0.710 ± 0.045	0.948 ± 0.004	0.968 ± 0.022	-	1	1
Br	35	11.91	0.741 ± 0.046	0.953 ± 0.004	0.974 ± 0.022	0.871	1	1
Rb	37	13.38	0.796 ± 0.029	0.962 ± 0.005	0.984 ± 0.023	-	1	1
Sr	38	14.14	0.823 ± 0.037	0.966 ± 0.005	0.988 ± 0.023	-	1	1
Ag	47	22.10	0.988 ± 0.045	0.997 ± 0.005	1	0.996	1	1
In	49	24.14	1.012 ± 0.049	1.002 ± 0.005	1	1.003	1	1
Sn	50	25.19	1.023 ± 0.049	1.005 ± 0.005	1	1.004	1	1
Sb	51	26.27	1.032 ± 0.049	1.007 ± 0.005	1	1.006	1	1
Te	52	27.38	1.042 ± 0.049	1.008 ± 0.005	1	1.009	1	1
Ba	56	32.06	1.073 ± 0.048	1.020 ± 0.005	1	1.016	1	1
La	57	33.30	1.079 ± 0.048	1.021 ± 0.005	1	-	1	1
Ce	58	34.56	1.084 ± 0.049	1.023 ± 0.005	1	-	1	1
Pr	59	35.86	1.089 ± 0.048	1.024 ± 0.005	1	-	1	1
Nd	60	37.18	1.095 ± 0.047	1.025 ± 0.006	1	1.019	1	1

Table 3.7 Continued

Tabulation of Values for $\omega_K(Z)/\omega_K(\text{Cd})$, $[1 + K\beta/K\alpha(Z)]/[1 + K\beta/K\alpha(\text{Cd})]$,
 $T_{K\alpha}(Z)/T_{K\alpha}(\text{Cd})$ and $A_{K\alpha}(Z)/A_{K\alpha}(\text{Cd})$

Element	Z	$E_{K\alpha}(Z)$ (1) keV	$\frac{\omega_{K\alpha}(Z)}{\omega_{K\alpha}(\text{Cd})}$ (2)	$\frac{[1 + K\beta/K\alpha(Z)]}{[1 + K\beta/K\alpha(\text{Cd})}]$ (3)	$\frac{T_{K\alpha}(Z)}{T_{K\alpha}(\text{Cd})}$ (4)	$\frac{A_{K\alpha}(Z)}{A_{K\alpha}(\text{Cd})}$ (5)
			Ge(Li) (a)	Si(Li) (b)		
Sm	62	39.91	1.105 ± 0.047	1.028 ± 0.006	1	1.021
Eu	63	41.31	1.108 ± 0.042	1.029 ± 0.006	1	1
Gd	64	42.75	1.112 ± 0.047	1.030 ± 0.006	1	1.021
Er	68	48.80	1.125 ± 0.046	1.035 ± 0.006	1	1.023
Yb	70	52.01	1.131 ± 0.046	1.037 ± 0.006	1	1.023
Pt	78	66.20	1.146 ± 0.043	1.048 ± 0.006	1	1.025
Pb	82	74.16	1.152 ± 0.043	1.054 ± 0.006	1	1.025
Bi	83	76.25	1.155 ± 0.043	1.056 ± 0.006	1	1.025

(1) Average K α X-ray energies, $E_{K\alpha}$, taken from the compilation of Storm and Israel (SI70); $E_{K\alpha}(\text{Cd}) = 23.11$ keV.

(2) K-shell fluorescence yields, ω_K , taken from the compilation of Bambynek, Crasemann, Fink, et. al. (BCF72); $\omega_K(\text{Cd}) = 0.840 \pm 0.029$; (cf. Section 1.1.3).

(3) K-shell radiative transition probability ratios, $K\beta/K\alpha$, taken from the compilation of Nelson, Saunders and Salem (NSS70); $K\beta/K\alpha(\text{Cd}) = 0.216 \pm 0.004$; (cf. Section 1.1.4).

(4) K α X-Ray fractional target transmission, T, in the lens tissue targets; $T(\text{Cd}) = 1$. See Appendix B for description of measurements.

(5) K α X-Ray absorption correction, A, calculated using the attenuation coefficients of Storm and Israel (SI70) and the National Bureau of Standards (NBS69).

(a) for path consisting of 0.051 mm mylar, 38.6 cm air, 0.13 mm Be and $40.4 \mu\text{g}/\text{cm}^2$ Au; $A(\text{Cd}) = 0.965$;

(b) for path consisting of 0.025 mm Be; $A(\text{Cd}) = 1$.

Table 3.8

Relative Intrinsic Detection Efficiencies [$\epsilon_{K\alpha}(Z)/\epsilon_{K\alpha}(Cd)$]
of the Ge(Li) and Si(Li) Detectors for K α X-Rays

Element	Z	keV	$E_{K\alpha}(Z)^{(1)}$	System C: Ge(Li) ⁽²⁾	System D: Si(Li) ⁽³⁾
				$\frac{\epsilon_{K\alpha}(Z)}{\epsilon_{K\alpha}(Cd)}$	$\frac{\epsilon_{K\alpha}(Z)}{\epsilon_{K\alpha}(Cd)}$
V	23	4.95		-	1.60 \pm 0.13
Cr	24	5.41		-	1.60 \pm 0.13
Mn	25	5.90		-	1.60 \pm 0.13
Fe	26	6.40		-	1.60 \pm 0.13
Co	27	6.93		-	1.60 \pm 0.13
Ni	28	7.47		-	1.60 \pm 0.13
Cu	29	8.04		-	1.60 \pm 0.13
Zn	30	8.63		-	1.60 \pm 0.13
As	33	10.53		-	1.60 \pm 0.13
Se	34	11.21		-	1.60 \pm 0.13
Br	35	11.91	0.914 \pm 0.041	1.60 \pm 0.13	1.60 \pm 0.13
Rb	37	13.38		-	1.60 \pm 0.13
Sr	38	14.14		-	1.58 \pm 0.12
Ag	47	22.10	0.996 \pm 0.032	1.082 \pm 0.010	1.082 \pm 0.010
In	49	24.14	1.003 \pm 0.028	0.931 \pm 0.005	0.931 \pm 0.005
Sn	50	25.19	1.008 \pm 0.026	0.855 \pm 0.009	0.855 \pm 0.009
Sb	51	26.27	1.012 \pm 0.023	0.783 \pm 0.011	0.783 \pm 0.011
Te	52	27.38	1.017 \pm 0.021	0.711 \pm 0.013	0.711 \pm 0.013
Ba	56	32.06	1.028 \pm 0.022	0.484 \pm 0.022	0.484 \pm 0.022
La	57	33.03	-	0.444 \pm 0.022	0.444 \pm 0.022
Ce	58	34.56	-	0.403 \pm 0.020	0.403 \pm 0.020
Pr	59	35.86	-	0.363 \pm 0.020	0.363 \pm 0.020
Nd	60	37.18	1.032 \pm 0.020	0.319 \pm 0.020	0.319 \pm 0.020
Sm	62	39.91	1.037 \pm 0.019	0.275 \pm 0.020	0.275 \pm 0.020
Eu	63	41.31	-	0.240 \pm 0.020	0.240 \pm 0.020
Gd	64	42.75	1.040 \pm 0.019	0.219 \pm 0.017	0.219 \pm 0.017
Er	68	48.80	1.040 \pm 0.018	0.163 \pm 0.015	0.163 \pm 0.015
Yb	70	52.01	1.040 \pm 0.018	0.126 \pm 0.013	0.126 \pm 0.013
Pt	78	66.20	0.993 \pm 0.020	-	-
Pb	82	74.16	0.928 \pm 0.023	-	-
Bi	83	76.25	0.912 \pm 0.027	-	-

(1) Average K α X-ray energies, $E_{K\alpha}$, taken from the compilation of Storm and Israel (SI70); $E_{K\alpha}(Cd) = 23.11$ keV.

(2) Relative intrinsic detection efficiencies, $\epsilon_{K\alpha}(Z)/\epsilon_{K\alpha}(Cd)$, of a 4.8 ± 0.2 mm Ge(Li) detector for K α X-rays. Calculated from the photoelectric absorption coefficients of Storm and Israel (SI70) and corrected for the Ge K X-ray escape peak probability using the experimental escape peak losses measured by Palms, Rao and Wood (PRW68). See Appendix D.

(3) Relative intrinsic detection efficiencies, $\epsilon_{K\alpha}(Z)/\epsilon_{K\alpha}(Cd)$, of a 1.7 ± 0.2 mm Si(Li) detector for K α X-rays. Calculated from the photoelectric absorption coefficients of Storm and Israel (SI70). See Appendix D.

measurements. The total uncertainties were typically of the order 2-6%.

The transition probability ratios $K\beta/K\alpha$, used to obtain the values $[1 + K\beta/K\alpha(Z)]/[1 + K\beta/K\alpha(Cd)]$, were taken from the compilation of Nelson, Saunders and Salem (NSS70) [cf. Section 1.1.4]. They estimated the errors in their tabulated values to be about 2% on each $K\beta/K\alpha$ value. The propagated errors on the $[1 + K\beta/K\alpha(Z)]/[1 + K\beta/K\alpha(Cd)]$ terms are therefore about 0.5%.

The fractional target transmission, the ratio of the intensity I_t of X-rays transmitted through the target to the intensity I_p of X-rays produced in the target, is given by (MFH70)

$$T = \frac{I_t}{I_p} = \frac{\cos \phi}{\mu_{abs} t} [1 - \exp(-\mu_{abs} t/\cos \phi)] , \quad (3.4)$$

where ϕ is the angle between the target normal and the distant detector, μ_{abs} is the total absorption coefficient for $K\alpha$ X-rays in the target, and t is the target thickness. The product $\mu_{abs} t$ for $K\alpha$ X-rays of element Z in 13 different Z/Cd lens tissue targets was measured (see Appendix B) by a series of transmission measurements. These values of $\mu_{abs} t$ were then used to calculate $T_{K\alpha}(Z)$ for the Z/Cd targets. The self-absorption became negligible ($T \approx 1.$) for elements greater than $Z \sim 40$, while the correction was about 20% ($T \approx 0.8$) at $Z \sim 25$. It was found that the values of $T_{K\alpha}(Z)$ as a function of Z could be well represented by a smooth regular curve drawn through the measured data points (see Figure B.1 in Appendix B). The maximum deviation of any of the measured values from the curve was 1.6%. Since $T_{K\alpha}(Cd) \approx 1.$, the values

for $T_{K\alpha}(Z)/T_{K\alpha}(\text{Cd})$ listed in Table 3.7 were obtained directly from the curve for $T_{K\alpha}(Z)$. The error limits on the ratio was taken to be approximately $\pm 2.5\%$.

The absorption correction $A_{K\alpha}(Z)$, the ratio of the transmitted $K\alpha$ X-ray intensity I to the original intensity I_0 of $K\alpha$ X-rays of element Z from the target is given by

$$A_{K\alpha}(Z) = \frac{I}{I_0} = \exp \left[-\sum_i \mu_i x_i \right] , \quad (3.5)$$

where μ_i is the attenuation coefficient for $K\alpha$ X-rays in the i th absorber, x_i is the thickness of i th absorber, and where the summation is over all i absorbers in the X-ray path interposed between the target and X-ray detector. For System C, the absorbers in the X-ray path to the Ge(Li) detector consisted of 0.051 mm Mylar, 38.6 cm air, 0.13 mm beryllium and $40.4 \mu\text{g}/\text{cm}^2$ gold (see Section 2.3.2). The only absorber in the X-ray path of System D was the 0.025 mm Be window on the Si(Li) detector (see Section 2.3.3). The total narrow beam photon cross sections* of Storm and Israel (SI70) were used to calculate the $K\alpha$ X-ray attenuation by the beryllium and gold. The air attenuation was calculated using the mass attenuation coefficients† of the National Bureau of Standards (NBS69) and assuming the standard air density of $1.293 \text{ mg}/\text{cm}^3$. The attenuation by the Mylar was approximated using mass

*The total narrow beam cross section as defined by Storm and Israel (SI70) consists of the sum of the total photoelectric, total pair production, total incoherent scattering from bound electrons, and coherent scattering cross sections.

†Coefficients are "Total with Coherent Scattering" (NBS69).

attenuation coefficients[†] (NBS69) for lucite combined with the density (1.39 g/cm³) of Mylar. Because of the similar composition of lucite [(C₅H₈O₂)_n] and Mylar [(C₅H₄O₂)_n], this should be a reasonable approximation. The ratios of the calculated absorption correction for element Z to that for Cd, A_{Kα}(Z)/A_{Kα}(Cd), are provided in Table 3.7 for both Systems C and D. For the most part, these corrections are very small and as a result their uncertainties are negligible.

Relative intrinsic detection efficiencies for both detectors were calculated from

$$\frac{\varepsilon_{K\alpha}(Z)}{\varepsilon_{K\alpha}(Cd)} = \left[\frac{1 + R(Cd K\alpha)}{1 + R(Z K\alpha)} \right] \left\{ \frac{1 - \exp[-\mu_{K\alpha}(Z)t]}{1 - \exp[-\mu_{K\alpha}(Cd)t]} \right\} , \quad (3.6)$$

where R(Z K α) and R(Cd K α) are the escape peak corrections for element Z and Cd K α X-rays, respectively, $\mu_{K\alpha}(Z)$ and $\mu_{K\alpha}(Cd)$ are the appropriate absorption coefficients for element Z and Cd K α X-rays respectively, and t is the real detector thickness (see Appendix D). The absorption coefficients, $\mu_{K\alpha}$, of Storm and Israel (SI70) were used for the calculations. For the Ge(Li) detector, and for the Si(Li) detector up to 60 keV, total energy absorption coefficients* were used. Above 60 keV, the calculations for the Si(Li) detector used photoelectric absorption coefficients. The escape peak corrections, R, for the Ge(Li) detector were taken from the measurements of Palms, Venugopala Rao and Wood (PRW68).

[†]Coefficients are "Total with Coherent Scattering" (NBS69).

*The total energy absorption photon cross section as defined by Storm and Israel (SI70) consists of the sum of the photoelectric absorption, pair production absorption and incoherent scattering from bound electron cross sections.

and Campbell and McNelles (CM72). These experimental escape peak losses are adequately predicted by both the theoretical estimate of the Axel model (A53) and by rigorous Monte Carlo calculations (ILS71). As described in Appendix D, the escape peak corrections, R, for the Si(Li) detector are negligible. The real detector thicknesses, t, were obtained from absolute and relative efficiency measurements with ^{57}Co , ^{109}Cd and ^{241}Am sources (see Appendix D). The absolute efficiencies were made in comparison to a standard 3" x 3" NaI(Tl) detector using Heath (H64) NaI efficiency calculations. The thicknesses are 1.7 ± 0.2 mm for the Si(Li) detector and 4.8 ± 0.2 mm for the Ge(Li) detector. Although the absolute efficiencies are very sensitive to the real detector thickness, the relative efficiencies defined by Equation 3.6 are not. The results of the efficiency calculations for both detectors are provided in Table 3.8. The error limits on the values of $\epsilon_{K\alpha}(Z)/\epsilon_{K\alpha}(\text{Cd})$ in the Table reflect the maximum deviations for a detector thickness uncertainty of 0.2 mm. These error limits are estimated to be greater than 95% confidence limits (approximately two standard deviations) since they were derived from the extremes of the detector thickness uncertainty. The estimated errors on the values for the Ge(Li) detector also include the contributions from assuming a 25% uncertainty in the values of the escape peak losses, R. As indicated by the magnitude of the error bars, the relative efficiencies can be obtained rather precisely. This, of course, is only true for the limited energy range spanned by the calculation, i.e., from 5 keV to 52 keV for the Si(Li) detector and from 12 keV to 76 keV for the Ge(Li) detector.

The values of the various terms in Table 3.7 and 3.8 were combined as given by Equation 3.3 with the relative $K\alpha$ X-ray yields, $\gamma_{K\alpha}(Z)$, to obtain the relative K-shell ionization cross sections, $\sigma_K(Z)/\sigma_K(Cd)$. The results for the two sets of measurements are listed in Table 3.9. The estimated error limits which are also listed were obtained from a quadratic propagation of the uncertainties on the values for $\gamma_{K\alpha}(Z)$, $\omega_K(Z)/\omega_K(Cd)$, $[1 + K\beta/K\alpha(Z)]/[1 + K\beta/K\alpha(Cd)]$, $T_{K\alpha}(Z)/T_{K\alpha}(Cd)$ and $\epsilon_{K\alpha}(Z)/\epsilon_{K\alpha}(Cd)$. As indicated, the overall uncertainties (> 95% confidence limits) are typically 7-10% for System C and 7-13% for System D. In the cases where comparisons are possible the two measurements are in good agreement. These experimental results are also compared to theoretical relative K-shell ionization cross sections, $\sigma_K(Z)/\sigma_K(Cd)$, calculated by the Kolbenstvedt theory (K67) [cf. Section 1.1.2]. The calculations were made using experimental K-shell critical absorption X-ray energies (FH55) for the K-shell ionization energy. The theoretical cross section for Cd used to normalize the others is $\sigma_K(Cd) = 48.3$ barns. These theoretical relative cross sections are also listed in Table 3.9. In figure 3.7, both sets of the experimental measurements are displayed and compared to the results of the Kolbenstvedt theory. As shown, the theoretical values are in excellent agreement with the experimental values in the $Z \sim 50$ region. At higher Z , the theoretical values tend to be slightly high; and in the low Z region ($Z < 40$), they are too low. The trends of the present results appear to agree with prior experimental measurements (refer to Table 1.1). The only two previous cross section measurements at 2 MeV are those

Table 3.9

Comparison of Experimental and Theoretical Relative K-Shell Ionization Cross Sections [$\sigma_K(Z)/\sigma_K(Cd)$] for 2 MeV Electrons

Element	Z	keV	I _K (Z)*	Experimental $\sigma_K(Z)/\sigma_K(Cd)$		Kolbenstvedt (K67) Theory [†] $\sigma_K(Z)/\sigma_K(Cd)$
			System C: Ge(Li)	System D: Si(Li)		
V	23	5.46	-	7.69 ± 0.83		5.82
Cr	24	5.99	-	5.89 ± 0.63		5.26
Mn	25	6.54	-	5.88 ± 0.75		4.78
Fe	26	7.11	-	5.56 ± 0.59		4.35
Co	27	7.71	-	5.23 ± 0.66		3.98
Ni	28	8.33	-	5.10 ± 0.63		3.64
Cu	29	8.98	-	4.32 ± 0.46		3.35
Zn	30	9.66	-	4.00 ± 0.49		3.11
As	33	11.86	-	2.93 ± 0.35		2.46
Se	34	12.65	-	2.43 ± 0.31		2.30
Br	35	13.48	2.17 ± 0.21	2.57 ± 0.30		2.15
Rb	37	15.20	-	2.23 ± 0.23		1.88
Sr	38	16.11	-	1.94 ± 0.20		1.76
Ag	47	25.52	1.21 ± 0.10	1.26 ± 0.091		1.052
In	49	27.93	0.953 ± 0.075	0.937 ± 0.069		0.950
Sn	50	29.19	0.944 ± 0.073	0.936 ± 0.069		0.905
Sb	51	30.49	0.920 ± 0.070	0.877 ± 0.065		0.861
Te	52	31.81	0.820 ± 0.062	0.830 ± 0.062		0.822
Ba	56	37.41	0.668 ± 0.050	0.650 ± 0.055		0.683
La	57	38.93	-	0.409 ± 0.035		0.654
Ce	58	40.45	-	0.501 ± 0.044		0.625
Pr	59	42.00	-	0.513 ± 0.046		0.600
Nd	60	43.57	0.482 ± 0.035	0.458 ± 0.043		0.576
Sm	62	46.85	0.469 ± 0.034	0.430 ± 0.043		0.530
Eu	63	48.52	-	0.457 ± 0.049		0.509
Gd	64	50.23	0.457 ± 0.033	0.448 ± 0.047		0.489
Er	68	57.48	0.390 ± 0.028	0.332 ± 0.038		0.418
Yb	70	61.30	0.352 ± 0.025	0.314 ± 0.039		0.389
Pt	78	78.38	0.255 ± 0.018	-		0.294
Pb	82	88.00	0.214 ± 0.015	-		0.257
Bi	83	90.52	0.204 ± 0.015	-		0.248

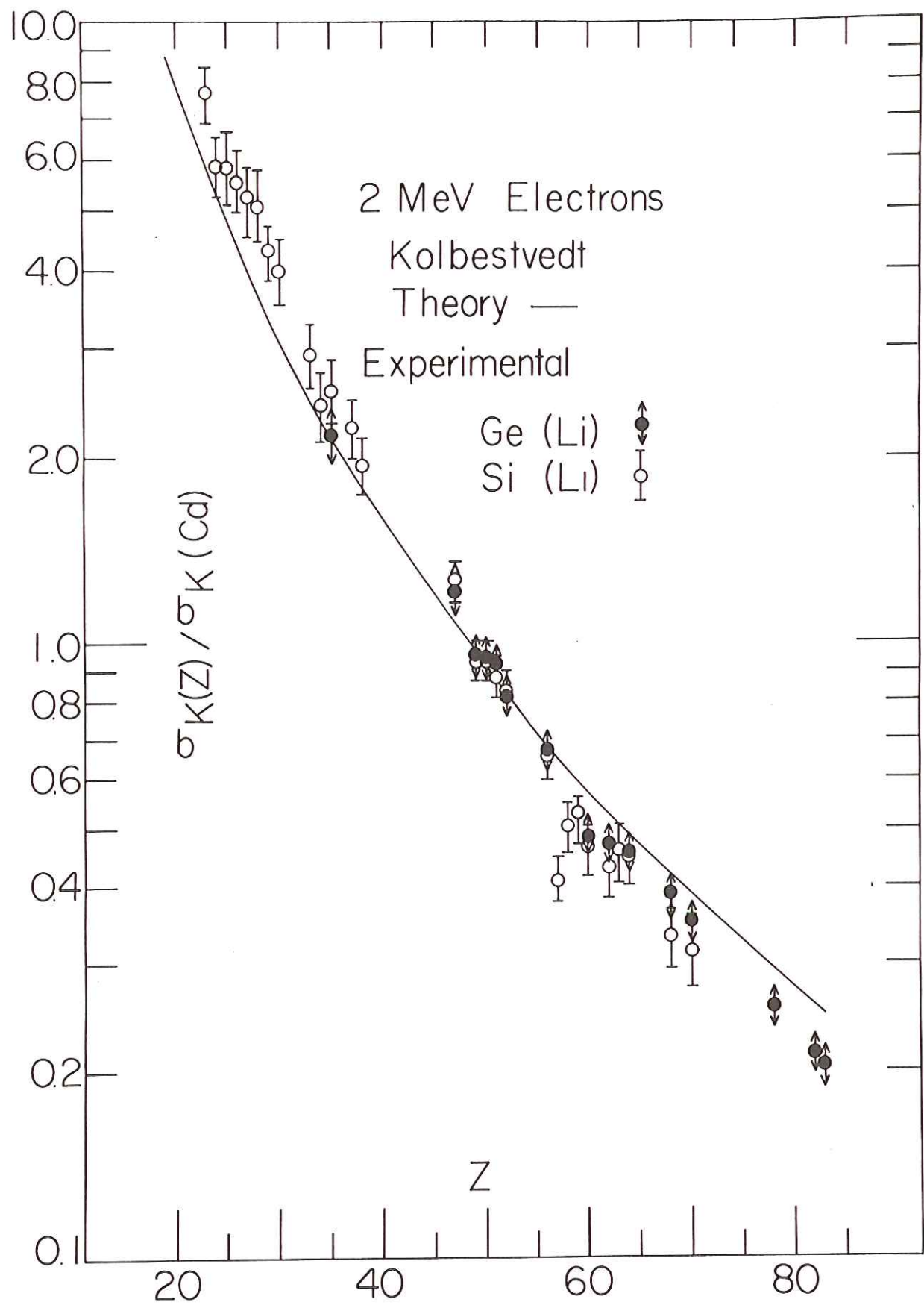
*Experimental K-shell critical absorption X-ray energies taken from the compilation of Fine and Hendee (FH55); I_K(Cd) = 26.71 keV.

†Calculated using the tabulated I_K values for the K-shell ionization energy; σ_K(Cd) = 48.3 barns; (cf. Section 1.1.2).

FIGURE 3.7

Experimental and Theoretical Relative K-Shell
Ionization Cross Sections [$\sigma_K(Z)/\sigma_K(Cd)$]
as a Function of Atomic Number (Z)
for 2 MeV Electrons

The experimental values are those obtained from the present work with the Ge(Li) [System C] and Si(Li) [System D] detectors. The solid curve was calculated by Kolbenstvedt (K67) theory using experimental critical absorption energies (FH55) for the K-shell ionization energies.



for tin [$\sigma_K(\text{Sn}) = 44 \pm 4 \text{ b}$] and gold [$\sigma_K(\text{Au}) = 11 \pm 1 \text{ b}$] measured by Rester and Dance (RD66). The value of 43.7 b for tin calculated by Kolbenstvedt theory is in excellent agreement with Rester and Dance's measurement, while the theoretical value for gold (13.7 b) is too high by $\sim 25\%$. This same trend, i.e., that the Kolbenstvedt theory predicts slightly higher cross sections at high Z, was also found in the present work.

The absolute cross section measurement of Rester and Dance for tin at 2 MeV, $\sigma_K(\text{Sn})$, can be used to obtain an absolute cross section for cadmium, $\sigma_K(\text{Cd})$, from the measured relative cross section for tin, $\sigma_K(\text{Sn})/\sigma_K(\text{Cd})$. Using this value for cadmium, all of the relative cross sections, $\sigma_K(Z)/\sigma_K(\text{Cd})$, listed in Table 3.9 can be converted into absolute cross sections, $\sigma_K(Z)$. These results are given in Table 3.10 and compared to the values calculated by the Kolbenstvedt theory. The percent differences in the theoretical cross sections from the experimental measurements are also provided to show the systematic deviation in the two sets. In the region around $Z \sim 50$, the agreement is within $\sim 5\%$, while at both higher and lower Z, the discrepancies are as large as 20-30%. In general, the theoretical values of Kolbenstvedt (K67) are too high for the heavy elements (higher Z). This is also indicated by Rester and Dance's (RD66) measurement of gold at 2.0 MeV, and by the measurements of Berkner, Kaplan and Pyle (BKP70) for palladium and gold at energies of 2.5 and 7.1 MeV (see Table 1.1). In the light element region (low Z), the Kolbenstvedt theory predicts cross sections which are too low. There have been no previous experimental confirmations of this systematic deviation in the light elements.

Table 3.10

Comparison of Experimental and Theoretical K-Shell
Ionization Cross Sections for 2 MeV Electrons

Element	Z	Experimental* σ_K (barns)	Theoretical† σ_K (barns)	% Difference†
V	23	361 ± 53	281	- 22.
Cr	24	277 ± 41	254	- 7.9
Mn	25	276 ± 43	231	- 16.
Fe	26	261 ± 38	210	- 20.
Co	27	246 ± 40	192	- 22.
Ni	28	240 ± 38	176	- 27.
Cu	29	203 ± 30	162	- 20.
Zn	30	188 ± 30	150	- 20.
As	33	138 ± 21	119	- 14.
Se	34	114 ± 19	111	- 2.6
Br	35	111 ± 12	104	- 6.3
Rb	37	105 ± 15	90.7	- 14.
Sr	38	91.2 ± 13.1	85.0	- 6.8
Ag	47	57.8 ± 5.2	50.8	- 12.
Cd	48	46.8 ± 4.1	48.3	+ 3.2
In	49	44.2 ± 4.0	45.9	+ 3.8
Sn	50	(44 ± 4)	43.7	- 0.7
Sb	51	42.1 ± 3.7	41.6	- 1.2
Te	52	38.6 ± 3.4	39.7	+ 3.1
Ba	56	30.9 ± 2.8	33.0	+ 6.8
La	57	19.2 ± 2.5	31.6	+ 13.
Ce	58	23.6 ± 3.1	30.2	+ 28.
Pr	59	24.1 ± 3.2	29.0	+ 20.
Nd	60	22.0 ± 2.0	27.8	+ 26.
Sm	62	21.1 ± 2.0	25.6	+ 21.
Eu	63	21.5 ± 3.1	24.6	+ 14.
Gd	64	21.2 ± 2.0	23.6	+ 6.7
Er	68	16.9 ± 1.6	20.2	+ 20.
Yb	70	15.6 ± 1.6	18.8	+ 21.
Pt	78	11.9 ± 1.5	14.2	+ 19.
Au	79	(11 ± 1)	13.7	+ 25.
Pb	82	10.0 ± 1.2	12.4	+ 24.
Bi	83	9.5 ± 1.2	12.0	+ 26.

*Obtained from the relative K-shell ionization cross section measurements (Table 3.9) assuming an absolute cross section of 44 ± 4 barns for Sn as measured by Rester and Dance (RD66). Their measured value for Au is also listed, $\sigma_K(\text{Au}) = 11 \pm 1$.

†Calculated by Kolbenstvedt (K67) theory using experimental K-shell critical absorption energies (FH55) for the K-shell ionization energy.

$$\frac{\sigma_K(\text{theoretical}) - \sigma_K(\text{experimental})}{\sigma_K(\text{experimental})} \times 100\%$$

The Kolbenstvedt theory is in good approximate agreement ($\pm 25\%$) with the experimental cross sections over the entire periodic range of elements from $Z = 23$ to $Z = 83$. This is a surprising result since numerous approximations were made in the derivation of the theoretical formulae for ease of computation. It is quite likely that the remaining gross systematic deviation in the theory for both low and high Z regions may be removed by re-evaluating the computational approximations. That is, the underlying assumptions of the theory [cf. Section 1.1.2] may prove to be adequate if the derivation is carried out with more rigor. This view of course assumes that the K-shell ionization cross sections vary smoothly as a function of atomic number. The relative cross sections measured in these studies suggests that there are irregularities in the Z dependence on the cross sections. The most apparent is at $Z \approx 60$. As shown in Figure 3.7, both sets of measurements indicate an abrupt change in the slope of the data in this region. Although the uncertainties in the measurements are too large to make a strong case for the deviations from one element to the next, the general trend was duplicated in both sets of independent measurements. Since this trend does not rely on the absoluteness of any one single measurement which may be in error, the effect appears to be real. The subtlety of this effect however, demands much more precise measurements. Furthermore, a theoretical description of these irregularities will require a very realistic quantum mechanical calculation unlike the simplistic theory of Kolbenstvedt.

Part 4

CONCLUSIONS

Two interrelated experimental studies were pursued in this work. The first was to demonstrate the use and capability of high energy electron impact ionization for elemental analysis by energy dispersive X-ray spectrometry. The second was to make a critical evaluation of the Kolbenstvedt (K67) theory for K-shell ionization by relativistic electrons. Both of these efforts, which are summarized and discussed in the following two sections, have successfully fulfilled their objectives. Hopefully, the results and conclusions of this thesis will provide the incentive and proper direction for further study.

4.1 Application to Elemental Analysis

It was demonstrated that high energy electron impact ionization has some distinct advantages over other methods used for elemental analysis by X-ray spectrometry. These advantages are characterized by the large range of MeV electrons in solids with a consequent small energy loss in thin samples, and by the smooth variation of the K-shell ionization cross section with both atomic number and electron energy. As a result, the method can simultaneously detect or determine all elements over a wide range with comparable sensitivity. Like any other analytical method, high energy electron impact ionization is not ideal for all applications, but it is a viable complement to the existing methods.

The method developed for this work is simple, fairly rapid and requires only a minimum of sample preparation and data analysis. It was

shown to be suitable for analysis of samples of completely unknown constituency and could easily be extended for routine analyses. The capability of the method for quantitative analysis was tested with three National Bureau of Standards metal alloy standards. In the assays of these three NBS samples, elements ranging from iron ($Z = 26$) to lead ($Z = 82$) and with concentrations ranging from 0.06% to 88% were quantitatively determined. In general, good approximate agreement with the reported assays was found. For even the minor constituents, the accuracy of the results were of the order of 5-10%. Several elements which were only present in small amounts were not detected in the present analyses because of the proximity of intense X-ray lines from nearby elements. However, the intent of these studies was to demonstrate only the potential of the new method. No effort was made to obtain the highest possible precision and accuracy, or to achieve the ultimate detection sensitivity. It should be evident that extensive improvements could be made by adopting the well known techniques used in conventional X-ray analysis. These may include use of critical absorbers, improved target preparation techniques and corrections for matrix effects. In the present work, the electron beam currents used were typically 100 nA and the detectors subtended solid angles of the order of 0.001. Since available accelerators can easily deliver a thousand times more current and since the solid angle factor can be increased, it should be possible to make use of higher resolution crystal spectrometers to improve the signal-to-noise ratio without incurring any loss of overall efficiency. Thus, one may anticipate for the future a manyfold increase in the

sensitivity and accuracy of elemental analysis by high energy electron impact ionization.

4.2 K-Shell Ionization Cross Sections

The major effort for the K-shell ionization cross section measurements was to establish the atomic number (Z) dependence on the cross section over a wide range of elements. Prior experimental measurements were performed for only a few elements and most of these were elements with $Z \geq 50$ [cf. Table 1.1]. The Kolbenstvedt (K67) theory was shown to be in reasonable agreement with the energy dependence of these cross section measurements. Although the absolute magnitudes of the theoretical cross sections were found to deviate by as much as 25% from the measured values, the general trend of the energy dependence is well represented by the Kolbenstvedt theory. Furthermore, in the 1-5 MeV range, the cross sections are fairly constant with energy, while they decrease rapidly with increasing atomic number at a given electron energy. Therefore, critical comparisons of the Kolbenstvedt theory to the Z dependence on the cross sections probably provides a more stringent test of the applicability of the theory.

Relative K-shell ionization cross sections of 31 elements from $Z = 23$ to $Z = 83$ for 2 MeV electrons were measured. In general, the Kolbenstvedt theory was found to be in good approximate agreement ($\pm 25\%$) with the measurements. In the medium Z region ($Z \approx 50$), the agreement is excellent, but systematic deviations were found in both low and high Z regions. The cross sections predicted by the Kolbenstvedt theory are systematically too small in the low Z region ($Z \lesssim 40$) and too

large in the high Z region ($Z \gtrsim 60$). This deviation in the heavy elements was observed in prior measurements for gold at 2 MeV (RD66) and also at 2.5 and 7.1 MeV (BKP70). The deviations in the opposite direction for the light elements was heretofore unknown.

The absolute cross section measurement of Rester and Dance (RD66) for tin at 2 MeV was combined with the present relative cross section measurements to obtain absolute cross sections for all 31 elements. In this way, the number of elements for which there are K-shell ionization cross sections in the energy range from 0.5 to 10.0 MeV has been increased fourfold. The reliability of these cross sections is, by necessity, dependent on the accuracy of Rester and Dance's absolute cross section measurement for tin. However, if a high precision measurement at 2 MeV for any of the 31 elements becomes available, then the absolute cross sections can be recalculated from the measured relative cross section data. All of the previous cross section measurements including those of the present work have been performed with thin solid samples. In extracting cross section data, corrections had to be made for target matrix effects, such as self-absorption of the X-rays in the target itself. To minimize these sources of uncertainty, it would be advantageous to prepare targets in the gaseous or vapor states over a wide range of elements. Since gases can be pressurized and rarefied with relative ease, the density of atoms can be chosen as to essentially eliminate the uncertainty due to multiple scattering of the electrons, self-excitation due to bremsstrahlung or secondary fluorescence, and self-absorption. Very high precision cross sections should be attainable in this way. These high precision measurements would be necessary

in verifying the seeming irregularities in the Z dependence on the K-shell ionization cross sections, as suggested in this work.

Part 5

LITERATURE CITED

- A53 P. Axel, "Escape Peak Correction to Gamma Ray Intensity Measurements Made with Sodium-Iodide Crystals", Brookhaven National Laboratory BNL Report No. 271 (T-44), 1953.
- ACS60 American Chemical Society, "Reagent Chemicals, American Chemical Society Specifications", 1960, p. 115.
- AM58 A. M. Arthurs and B. L. Moiseiwitsch, Proc. Roy. Soc. (London) A247, 550 (1958).
- B30 H. Bethe, Ann. Physik 5, 325 (1930).
- B35 E. H. S. Burhop, Proc. Roy. Soc. (London) A148, 272 (1935).
- B40 E. H. S. Burhop, Proc. Cambridge Phil. Soc. 36, 43 (1940).
- B55 E. H. S. Burhop, J. Phys. Radium 16, 625 (1955).
- B63 L. S. Birks, "Electron Probe Microanalysis", Interscience, N. Y., 1963.
- B69 L. S. Birks, "X-Ray Spectrochemical Analysis", Second Edition, Interscience, N. Y., 1969.
- BCF72 W. Bambynek, B. Crasemann, R. W. Fink, H. U. Freund, Hans Mark, C. D. Swift, R. E. Price and P. Venugopala Rao, "X-Ray Fluorescence Yields and Coster-Kronig Transition Probabilities", to be published, 1972.
- BKP70 K. H. Berkner, S. N. Kaplan and R. V. Pyle, Bull. Amer. Phys. Soc. 15, 786 (1970).
- BS64 M. J. Berger and S. M. Seltzer, "Tables of Energy Losses and Ranges of Electrons and Positrons" in "Studies in Penetration of Charged Particles in Matter", National Academy of Sciences - National Research Council, NAS-NRC Publication No. 1133, Nuclear Science Series Report No. 39, Washington, D. C., 1964, p. 205.
- C63 E. J. Callen, Rev. Mod. Phys. 35, 524 (1963); "Role of Atomic Electrons in Nuclear Transformations", Vol. 3, Nuclear Energy Information Center, Warsaw, 1963, p. 419.
- C68 L. A. Currie, Anal. Chem. 40, 586 (1968).
- CA35 A. H. Compton and S. K. Allison, "X-Rays in Theory and Experiment", Second Edition, Van Nostrand, N. Y., 1935.

- CM60 M. R. Cleland and K. H. Morganstern, IRE Trans. Ind. Elect. IE-7, No. 2, 36 (1960).
- CM72 J. L. Campbell and L. A. McNelles, Nucl. Instr. and Meth. 98, 433 (1972).
- COM71 J. L. Campbell, P. O'Brien and L. A. McNelles, Nucl. Instr. and Meth. 92, 269 (1971).
- CS35 E. U. Condon and G. H. Shortley, "The Theory of Atomic Spectra", Cambridge Univ. Press, Cambridge, 1935, p. 316 ff.
- D28 C. G. Darwin, Proc. Roy. Soc. (London) A118, 654 (1928).
- E55 R. D. Evans, "The Atomic Nucleus", McGraw-Hill, N. Y., 1955.
- FH55 S. Fine and C. F. Hendee, Nucleonics 13, No. 3, 36 (1955).
- FJM66 R. W. Fink, R. C. Jopson, Hans Mark and C. D. Swift, Rev. Mod. Phys. 38, 513 (1966).
- G57 G. W. Grodstein, National Bureau of Standards Circular 583, U. S. Dept. of Commerce, Washington, D. C. (1957).
- G62 J. W. Gofman, Adv. Biol. Med. Phys. 8, 1 (1962); J. W. Gofman, O. deLalla, G. Johnson, E. L. Kovich, O. Lowe, W. Martin, D. L. Piluso, R. K. Tandy, F. Upham, R. Weitzel and D. Wilbur, "Chemical Elements of the Blood of Man", Univ. California Radiation Laboratory Rpt. UCRL-9897, 1962.
- G72 J. M. Given, Jr., Fisher Scientific Co., Rochester, N. Y., private communication, 1972.
- GB72 R. W. Gould and S. R. Bates, X-Ray Spectrometry 1, 29 (1972).
- H54 W. Heitler, "The Quantum Theory of Radiation", Third Edition, Oxford Univ. Press, 1954.
- H58 D. Halliday in "Handbook of Physics", E. U. Condon and H. Odishaw (Editors), McGraw-Hill, N. Y., 1958, p. 9-141.
- H64 R. L. Heath, "Scintillation Spectrometry: Gamma-Ray Spectrum Catalog", Vol. 1, Second Edition, AEC Research and Development Rpt. IDO-16880-1, Physics, TID-4500, 1964.
- H72 J. H. Head, Nucl. Instr. and Meth. 98, 419 (1972).
- HFF70 J. S. Hansen, H. U. Freund and R. W. Fink, Nucl. Phys. A142, 604 (1970).
- HWF64 H. Hansen, H. Weigmann and A. Flammersfeld, Nucl. Phys. 58, 241 (1964).

- ILS71 H. I. Israel, D. W. Lier and E. Storm, Nucl. Instr. and Meth. 91, 141 (1971).
- J62 J. D. Jackson, "Classical Electrodynamics", Wiley, N. Y., 1962.
- JAJ70 T. B. Johansson, R. Akelsson and S. A. Johansson, Nucl. Instr. and Meth. 84, 141 (1970).
- JW66 J. F. W. Jensen and A. H. Wapstra in "Internal Conversion Processes", J. H. Hamilton (Editor), Academic Press, N. Y., 1966, p. 237.
- K65 H. Kaiser, Z. Anal. Chem. 209, 1 (1965).
- K67 H. Kolbenstvedt, J. Appl. Phys. 38, 4785 (1967).
- K69 L. J. Kieffer, Atomic Data 1, 19 (1969); erratum: 1, 359 (1970).
- KB64 J. F. Kircher and R. E. Bowman (Editors), "Effects of Radiation on Materials and Components", Reinhold, N. Y., 1964.
- KCC71 V. O. Kostroun, M. H. Chen and B. Grasemann, Phys. Rev. A3, 533 (1971).
- KD66 L. J. Kieffer and G. H. Dunn, Rev. Mod. Phys. 38, 1 (1966).
- KM59 H. W. Koch and J. W. Motz, Rev. Mod. Phys. 31, 920 (1959).
- KS52 I. M. Kolthoff and E. B. Sandell, "Textbook of Quantitative Inorganic Analysis", Third Edition, MacMillan, 1952, p. 457.
- L30 A. E. Lindh, "Röntgenspektroskopie, Handbuch der Experimental physik", Vol. 24, Akademische Verlagsgesellschaft M. B. H., Leipzig, 1930.
- L62 M. A. Listengarten, Izv. Akad. Nauk. SSSR, Ser. Fiz. 26, 182 (1962) [Bull. Acad. Sci. USSR, Phys. Columbia Tech. Transl. 26, 182 (1962)]; Izv. Akad. Nauk. SSSR, Ser. Fiz. 25, 792 (1961) [Bull. Acad. Sci. USSR, Phys. Columbia Tech. Transl. 25, 803 (1961)].
- LSS72 A. Li-Scholz, W. Scholz, R. Collé and I. L. Preiss, to be published, 1972.
- LSW66 H. Leutz, K. Schneckenberger and H. Wenninger, Nucl. Phys. 63, 263 (1966).
- M32 C. Møller, Ann. Physik 14, 531 (1932).
- M62 W. J. Moore, "Physical Chemistry", Third Edition, Prentice-Hall, Englewood Cliffs, N. J., 1962.

- M70 E. J. McGuire, Phys. Rev. A2, 273 (1970).
- M72 R. O. Müller, "Spectrochemical Analysis by X-Ray Fluorescence", Plenum Press, N. Y., 1972.
- MB35 H. S. W. Massey and E. H. S. Burhop, Phys. Rev. 48, 468 (1935).
- MB69 H. S. W. Massey and E. H. S. Burhop, "Collisions of Electrons with Atoms", Vol. I of "Electronic and Ionic Impact Phenomena", Second Edition, Oxford Univ. Press, 1969.
- MFH70 L. M. Middleman, R. L. Ford and R. Hofstadter, Phys. Rev. A2, 1429 (1970).
- MM33 H. S. W. Massey and C. B. O. Mohr, Proc. Roy. Soc. (London) A140, 613 (1933).
- MM65 N. F. Mott and H. S. W. Massey, "The Theory of Atomic Collision", Third Edition, Oxford Univ. Press, 1965.
- MP64 J. W. Motz and R. C. Placious, Phys. Rev. 136, A662 (1964).
- NBS69 National Bureau of Standards, "Photon Cross Sections, Attenuation Coefficients and Energy Absorption Coefficients from 10 keV to 100 GeV", NSRDS-NBS Rpt. No. 29, U. S. Dept. of Commerce, Washington, D. C., 1969.
- NSS70 G. C. Nelson, B. G. Saunders and S. I. Salem, Atomic Data 1, 377 (1970).
- P60 H. S. Perlman, Proc. Phys. Soc. (London) 76, 623 (1960).
- PE68 Perkin-Elmer, "Analytical Methods for Atomic Absorption Spectrophotometry", Publication No. 990-9638, Revised Sept., 1968.
- PRW68 J. M. Palms, P. Venugopala Rao and R. E. Wood, Nucl. Instr. and Meth. 64, 310 (1968).
- RD66 D. H. Rester and W. E. Dance, Phys. Rev. 152, 1 (1966).
- RS55 R. A. Rubenstein and J. N. Synder, Phys. Rev. 97, 1653 (1955).
- S34 D. Graf Soden, Ann. Physik 19, 409 (1934).
- S57 A. E. Sandström in "Handbuch der Physik", S. Flügge (Editor), Band XXX, Springer-Verlag, Berlin, 1957, p. 78.
- S69 J. H. Scofield, Phys. Rev. 179, 9 (1969).

- SE69 V. W. Slivinsky and P. J. Ebert, Phys. Letters 29A, 463 (1969); UCRL Rpt. No. 71632, 1969 (unpublished).
- SI70 E. Storm and H. I. Israel, Nucl. Data A7, 565 (1970).
- VT69 L. Varnell and J. Trischuk, Nucl. Instr. and Meth. 76, 109 (1969).
- W33 E. H. S. Wetzel, Phys. Rev. 44, 25 (1933).
- W34 H. E. White, "Introduction to Atomic Spectra", McGraw-Hill, N. Y., 1934, p. 299 ff.
- WB71 D. L. Walters and C. P. Bhalla, Phys. Rev. A3, 519 (1971).
- WNL59 A. H. Wapstra, G. J. Nijgh and R. Van Lieshout, "Nuclear Spectroscopy Tables", North-Holland, Amsterdam, 1959, p. 80.

Part 6

APPENDICES

6.1 Appendix A

Silicon X-Ray Escape Peak Correction for Analysis of Iron
in Presence of Copper

6.2 Appendix B

Transmission Measurements for Target Self-Absorption
Corrections

6.3 Appendix C

Chemical Assay of $\text{CdCl}_2 \cdot 2\frac{1}{2}\text{H}_2\text{O}$ Reference Sample Reagent

6.4 Appendix D

Calculation of Relative Intrinsic Detection Efficiencies
for Si(Li) and Ge(Li) Detectors

APPENDIX A

Silicon X-Ray Escape Peak Correction for Analysis
of Iron in Presence of Copper

Silicon X-rays produced by photoelectric absorption of incident X-rays in a Si(Li) detector have a finite probability for escape from the detector crystal. Therefore, whenever X-rays of energy greater than the Si K-absorption edge (1.84 keV) are detected, the resultant spectrum contains escape peaks which arise from escape of the Si K X-rays. These escape peaks occur at an energy equal to the incident X-ray energy minus the energy of the Si K X-ray. For the Cu K_α X-ray (8.05 keV), the Si K_α X-ray (1.74 keV) escape peak occurs at 6.31 keV. Since this escape peak overlaps with the Fe K_α X-ray (6.40 keV), an analysis of the Fe K_α line in the presence of Cu must include a correction for the amount of Si X-ray escape.

The correction factor R is empirically defined by

$$R = \frac{N_{EP}}{N_{Cu}},$$

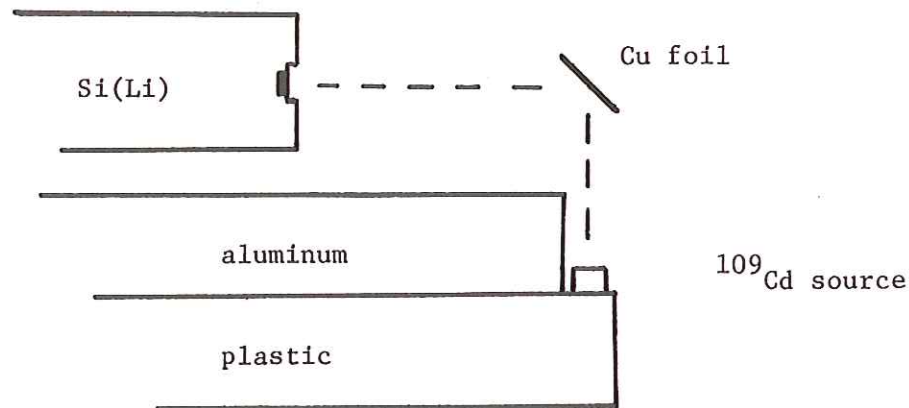
such that the size of the escape peak (N_{EP}) can be determined by a measurement of the number of Cu K_α X-rays (N_{Cu}) detected. With this definition, the number of Fe K_α X-rays can be unequivocally obtained from a measured sum peak ($N_{Fe} + N_{EP}$) using the measured N_{Cu} , i.e.

$$N_{Fe} = (N_{Fe} + N_{EP}) - RN_{Cu}.$$

The correction factor, so defined, is independent of the origin and devolution of the Cu X-ray before entering the detector. This is because the correction factor (or size of the escape peak) for a given

detector is determined relative to only the number of Cu K_α X-rays which are detected. It should also be relatively independent of geometry except for very large solid angles where edge effects may occur.

The correction factor R was measured by a "bench-top" fluorescence experiment using the same Si(Li) detector described in Section 2.3. The spectrometer consisted of the detector and preamplifier followed by a spectroscopy amplifier (Canberra 1417) which presented unipolar output pulses with a 2 μ sec shaping time constant and 93 Ω output impedance to a 1024-channel analyzer (Northern Scientific NS-600). The resolution of the spectrometer at 8.05 keV (Cu K_α) was 280 eV. Copper X-rays were produced by fluorescing a 0.038 mm thick Cu foil (1.5 x 1.9 cm) with a 10 mCi ¹⁰⁹Cd sealed source (New England Nuclear, X-ray excitation source NER-465). The source was shielded from the detector with aluminum and located at 90° to the detector axis at a distance of 4 cm from the foil. The center of the foil was located at



the intersection of the detector and source axes with its normal at 45° to both axes. This configuration is sketched above. Measurements were made with the foil at 6 and 12 cm from the detector. The resultant spectra were accumulated for 10.36 and 64.85 hours of livetime, respectively. A portion of the spectrum (Figure A.1) obtained at 12 cm shows the Cu K X-rays and the Si escape peak. A background spectrum accumulated for 10.35 hours in the 6 cm geometry was obtained without the foil in position. The background confirmed that the Cu and escape peaks were free of contaminants.

The Cu K_{α} and escape peaks were integrated using the procedure described in Section 2.4. The results for the correction factor at the two geometries are

$$R(6 \text{ cm}) = \frac{29630 \pm 2080}{4697700 \pm 6030} = 0.00631 \pm 0.00045 ,$$

and

$$R(12 \text{ cm}) = \frac{46160 \pm 3060}{7414700 \pm 6260} = 0.00623 \pm 0.00042 .$$

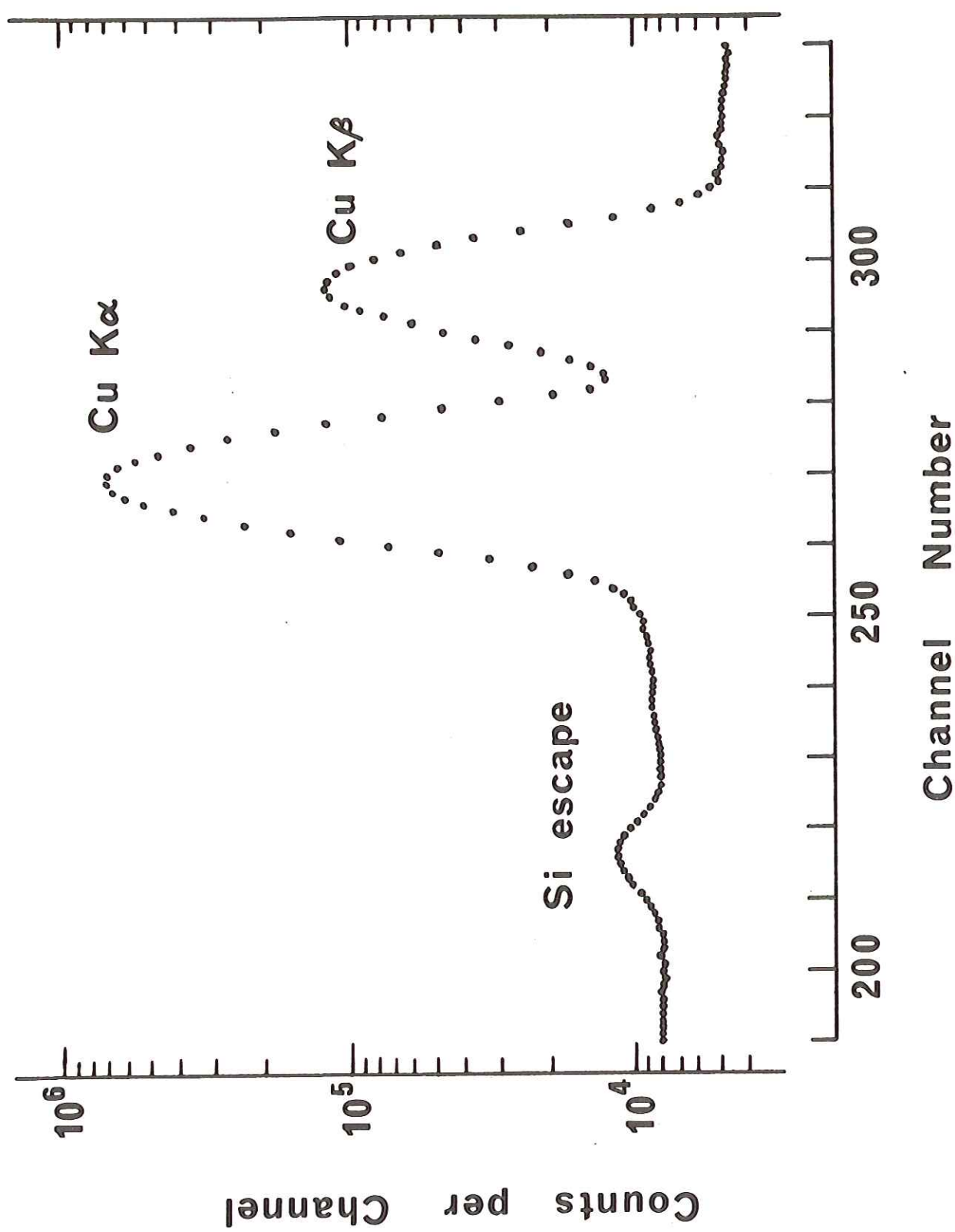
The major contribution to the error limits ($\sim 7\%$) was the uncertainty in locating the background under the escape peaks (see Section 2.4, Equation 2.1). Although the two geometries differed in solid angle by a factor of 4, the results are in remarkable agreement. The difference between the two measurements is 1.3% which is a factor of 5 smaller than the estimated uncertainties. The weighted (inverse square of the uncertainties) mean of the two measurements is

$$\bar{R} = \frac{N_{EP}}{N_{Cu}} = (6.27 \pm 0.31) \times 10^{-3} .$$

This value is probably reliable within the stated error limit (5%) for any solid angle smaller than the 6 cm geometry.

FIGURE A.1

X-Ray Spectrum of Cu K X-Rays Obtained with a Si(Li)
Detector Showing the Si K X-Ray Escape Peak



APPENDIX B

Transmission Measurements for Target Self-Absorption Corrections

A series of "bench-top" transmission measurements were made to obtain correction factors for the self-absorption of X-rays in the lens tissue targets. These measurements were made in a manner similar to the procedure used to obtain total broad-beam attenuation coefficients.* The intensity of a broad beam of $K\alpha$ X-rays was measured with and without an absorber (lens tissue target). The ratio of the intensity of the transmitted beam I to the intensity of the direct beam I_0 is related to the total attenuation coefficient μ and the absorber thickness t by the relation

$$\frac{I}{I_0} = \exp(-\mu t) . \quad (1)$$

By measuring the ratio I/I_0 in the transmission experiment, the product μt can be calculated and used to estimate the fractional target transmission T of X-rays produced uniformly in a target of thickness t and with a photoelectric absorption coefficient μ_{abs} . The intensity I_t of X-rays transmitted through the target is given by[†]

$$I_t = \int_0^{t/\cos \theta} I_x \exp[-\mu_{abs} \ell(x)] dx , \quad (2)$$

where $\ell(x)$ is the path length in the target for an X-ray produced at depth x , I_x is the uniform X-ray production intensity per unit length,

*G. W. Grodstein, National Bureau of Standards Circular 583, U. S. Department of Commerce, Washington, D. C. (1957).

[†]L. M. Middleman, R. L. Ford and R. Hofstadter, Phys. Rev. A2, 1429 (1970).

and θ is the angle between the incident electron beam direction and the normal to the target surface. Thus, the fractional target transmission is

$$T = \frac{I_t}{I_p} = \frac{\cos \phi}{\mu_{abs} t} [1 - \exp(-\mu_{abs} t/\cos \phi)] \quad (3)$$

where I_p is the total intensity of X-rays produced in the target and ϕ is the angle between the distant X-ray detector and the target normal.

For the transmission measurements, X-rays were produced by fluorescing thin targets of the desired element with a 10 mCi ^{109}Cd source using a configuration similar to that described in Appendix A. Targets of the various elements (about $2-4 \text{ cm}^2$) were held at a distance of 12.5 cm from the X-ray detector. The absorbers (lens tissue targets) were placed at a distance of 8.75 cm from the detector. With this arrangement, the X-ray beam as measured by the detector was incident on a $1-2 \text{ cm}^2$ area of the lens tissue. Care was taken to insure that the ^{109}Cd source was adequately shielded from the lens tissue. This was done to avoid fluorescence of the lens tissue by the ^{109}Cd source. The $K\alpha$ X-ray intensities of the direct beam I_0 and the transmitted beam I were measured with the same Si(Li) detector used for the ionization cross section measurements (see Section 2.3). This detector was employed for these "bench-top" measurements as described in Appendix A. The intensity measurements were made for 1000-4000 seconds of livetime, such that the statistical uncertainty on every intensity was less than 1-2%. The ratio I/I_0 was obtained from the intensity measurements for each X-ray target and absorber (lens tissue) pair. The statistical error (one standard deviation) on I/I_0 , σ_{I/I_0} , was obtained from

propagating the uncertainties on the foreground and background of both intensity measurements making the usual assumption of a Poisson distribution (i.e., $\sigma_N = \sqrt{N}$ where N is a measured foreground or background number). The exponential term μt and its estimated error was then calculated from I/I_0 and σ_{I/I_0} by

$$\mu t = \ln (I_0/I) \quad (4)$$

and

$$\sigma_{\mu t} = \frac{\sigma_{I/I_0}}{(I/I_0)} . \quad (5)$$

Substituting this value of μt for $\mu_{abs} t$ in Equation (3) and using the geometry for the cross section measurements (i.e. $\phi = 45^\circ$), the fractional transmission of X-rays produced in the target was estimated by

$$T = \frac{.70711}{\mu t} [1 - \exp(-\mu t/.70711)] . \quad (6)$$

The variance on this value of T is given by

$$\sigma_T^2 = \left[\frac{\exp(-\mu t/.70711) - T}{\mu t} \right]^2 \sigma_{\mu t}^2 . \quad (7)$$

The measurements were made on eighteen target element and absorber (lens tissue) pairs, ranging from vanadium ($Z = 23$) to antimony ($Z = 51$). The results of these measurements are provided in Table B.1. Uniformity of the lens tissues was checked by making the transmission measurements on two different areas of the absorber. No discernable differences were found in any of the several that were checked. As indicated by the results, the self-absorption in the lens tissue targets becomes negligible for elements greater than $Z \sim 40$, while the correction is about 20% at $Z \sim 25$. As seen in Figure B.1, the values of T for the thirteen Z/Cd targets as a function of Z can be well represented by a

smooth curve drawn through the data points. The maximum deviation of any measured value from this curve is less than 2%. The regularity of the curve is probably due to the similarity of the targets. That is, they have a rather constant thickness of approximately 1 mg/cm^2 , and the same Z/Cd atom ratio of about unity (see Section 2.2). Thus, the curve can be used to estimate the self-absorption (target transmission) of K α X-rays for any of the Z/Cd lens tissue targets.

Similar transmission measurements were made to determine the self-absorption of the Cu K α X-rays in the NBS metal alloy sample targets. The results are provided in Table B.2. In comparison to each other, the results are in good agreement with what one would predict from the target composition. That is, the Cu K α X-ray is more strongly absorbed in those targets containing Cd, or those with a higher content of heavy metals (e.g. NBS No. 54). The composition of these metal alloy samples and their respective targets is provided in Tables 2.4 through 2.7.

Table B.1
Transmission Measurements on Reference Sample Lens Tissue Targets

<u>Incident K_α X-Ray</u>	<u>Z</u>	<u>Absorber (Target)</u>	<u>I/I₀</u>	<u>μt</u>	<u>T</u>
V	23	V/Zn	0.9004 ± 0.0235	0.105	± 0.026
V	23	V/Cd	0.7476 ± 0.0115	0.291	± 0.015
Cr	24	Cr/Ni	0.9226 ± 0.0350	0.0806	± 0.0379
Cr	24	Cr/Cd	0.7417 ± 0.0227	0.299	± 0.031
Mn	25	Mn/Cd	0.7740 ± 0.0217	0.256	± 0.028
Fe	26	Fe/Cd	0.8287 ± 0.0134	0.188	± 0.016
Ni	28	Cr/Ni	0.9780 ± 0.0134	0.0222	± 0.0137
Ni	28	Ni/Cd	0.8673 ± 0.0142	0.142	± 0.016
Cu	29	Fe/Cd	0.8852 ± 0.0095	0.122	± 0.011
Cu	29	Cu/Cd	0.8863 ± 0.0091	0.121	± 0.010
Zn	30	V/Zn	0.9499 ± 0.0125	0.0514	± 0.0132
Zn	30	Zn/Cd	0.8844 ± 0.0181	0.123	± 0.021
As	33	As/Cd	0.9576 ± 0.0087	0.0433	± 0.0091
Se	34	Se/Cd	0.9635 ± 0.0048	0.0372	± 0.0050
Br	35	Rb/Br/Cd	0.9463 ± 0.0117	0.0552	± 0.0123
Rb	37	Rb/Br/Cd	0.9797 ± 0.0098	0.0206	± 0.0100
Sr	38	Sr/Cd	0.9699 ± 0.0109	0.0305	± 0.0112
Sb	51	Sb/Cd	1.0082 ± 0.0181	0.00820	± 0.0179

Table B.2
Transmission Measurements on NBS Metal Alloy Sample Lens Tissue Targets

<u>Incident K_a X-Ray</u>	<u>Absorber</u>	<u>I/I_o</u>	<u>T</u>		
Element	Z		μt		
Cu	29	NBS-52	0.9476 ± 0.0125	0.0538 ± 0.0132	0.963 ± 0.009
Cu	29	NBS-52/Cd	0.9108 ± 0.0122	0.0933 ± 0.0134	0.937 ± 0.009
Cu	29	NBS-54	0.9348 ± 0.0124	0.0674 ± 0.0133	0.954 ± 0.008
Cu	29	NBS-54/Cd	0.8519 ± 0.0116	0.1603 ± 0.0136	0.895 ± 0.008
Cu	29	NBS-63	0.9614 ± 0.0127	0.0393 ± 0.0132	0.973 ± 0.009
Cu	29	NBS-63/Cd	0.9144 ± 0.0122	0.0895 ± 0.0134	0.939 ± 0.009

solution which was assumed to be the primary standard for the procedure. As a consistency check, the AgNO_3 was also standardized against a known KCl solution and found to agree within the measurement precision. Three titrations on each of three $\text{CdCl}_2 \cdot 2\frac{1}{2}\text{H}_2\text{O}$ samples gave an assay of $81.6 \pm 0.3 \text{ CdCl}_2$ where the stated uncertainty is the maximum deviation of any of the six measurements from the mean.

The method used to determine Cd by atomic absorption analysis was the standard procedure prescribed by Perkin-Elmer* for their Model 303 spectrophotometer. The procedure employed the 2288 \AA Cd line from a hollow cathode lamp and an air-acetylene flame to atomize the sample. Sample solutions prepared from the $\text{CdCl}_2 \cdot 2\frac{1}{2}\text{H}_2\text{O}$ reagent were diluted and adjusted to about $1 \mu\text{g/ml}$ Cd for the absorbance measurements. Solutions containing the unknown ($\sim 1 \mu\text{g/ml}$ Cd) with standard additions of 0.5 and $1.0 \mu\text{g/ml}$ Cd were also prepared and measured. The CdCl_2 assay from measurements on two $\text{CdCl}_2 \cdot 2\frac{1}{2}\text{H}_2\text{O}$ samples was found to be 81.66 ± 0.04 .

The results from both methods are in agreement and it is conclusive that the manufacturers reported assay (80.5% CdCl_2) for the $\text{CdCl}_2 \cdot 2\frac{1}{2}\text{H}_2\text{O}$ is too low by 1.4%. Furthermore, the agreement suggests that the Cd content in the Cd metal reagent is 100%.

*Perkin-Elmer, Analytical Methods for Atomic Absorption Spectrophotometry, Publication No. 990-9638, Revised Sept., 1968.

APPENDIX D

Calculation of Relative Intrinsic Detection Efficiencies
for Si(Li) and Ge(Li) Detectors

The calculation of the relative intrinsic detection efficiencies for the Si(Li) and Ge(Li) detectors was described in Section 3.2. This appendix provides the justification for the algorithm of the calculation (see Equation 3.6) and the determination of the detector thicknesses.

If the counts in the full-energy peak are due solely to photoelectric interactions, then, for a parallel beam of photons incident on the normal of the detector, the photopeak efficiency is

$$\epsilon_{\text{photo}} = 1 - \exp [- (\mu_a / \rho)_\tau t] , \quad (1)$$

where $(\mu_a / \rho)_\tau$ is the photoelectric mass absorption coefficient for the detector material and t is the detector thickness. Fluorescent X-rays produced in the detector by photoelectric absorption of the incident photons have a finite probability for escape from the detector crystal. The photopeak efficiency given by Equation (1) does not consider this escape peak loss which depletes the photopeak intensity. If the escape peak loss is defined as the ratio of the escape peak intensity to the photopeak intensity, i.e.

$$R = \frac{I_{\text{escape}}}{I_{\text{photo}}} , \quad (2)$$

then the corrected efficiency is

$$\epsilon = \epsilon_{\text{photo}} / (1 + R) . \quad (3)$$

For thin detectors, Equation (3) has been shown to be a reasonable approximation to rigorous Monte Carlo efficiency calculations⁽¹⁾. For

thicker detectors, Equation (3) predicts lower efficiencies because some of the counts in the photopeak are due to non-photoelectric interactions, such as Compton scattering. Therefore, a part of the Compton attenuation coefficient should be added to the photoelectric coefficient. One possible choice is the total energy absorption coefficient⁽²⁾, $(\mu_a/\rho)_{en}$, which consists of the sum of the contributions from photoelectric absorption, pair production absorption and incoherent scattering (Compton) from bound electrons. The predicted efficiencies using $(\mu_a/\rho)_{en}$ in Equation (3) are in good agreement with Monte Carlo calculations at low energies, but they tend to be slightly higher at high energies⁽¹⁾. For the Ge(Li) detectors, the agreement is good up to approximately 100 keV; whereas, the results of the two calculations begin to diverge at \sim 60 keV with the Si(Li) detector. A reasonable compromise for the Si(Li) detector is to use $(\mu_a/\rho)_{en}$ coefficients up to 60 keV and the $(\mu_a/\rho)_T$ coefficients above 60 keV.

The K X-ray escape probability can be calculated using the model proposed by Axel⁽³⁾. For a "good" geometry, the probability for escape of K X-rays from the detector is given by

$$P(0^\circ) = \frac{1}{2}\omega_K k [1 - \Gamma \log (\frac{1 + \Gamma}{\Gamma})] , \quad (4)$$

with $\Gamma = \lambda_x/\lambda_\gamma$, where ω_K is the K-shell fluorescence yield, k is the probability that a photoelectric interaction will eject a K electron, and λ_x and λ_γ are the probability per unit distance of photoelectric absorption of the K X-rays and the incident photons, respectively. The escape peak losses for the Si(Li) detector are small in comparison to that for the Ge(Li) detector [refer to the discussion in Section 3.1]. This is a result of the low fluorescent yield of 0.047 for Si compared

to the value 0.540 for Ge⁽⁴⁾. At the K-edge, where the escape peak losses are largest, the correction R [Equation (2)] for the Si(Li) detector is less than 0.02, while R for the Ge(Li) detector is nearly 0.20⁽¹⁾. For both detectors, R decreases rapidly above their K-edges, but the large initial value and higher K-edge for Ge makes the losses significant up to 50 keV where R = 0.01 for the Ge(Li) detector. In comparison, the value of R \approx 0.01 is reached at 3 keV for the Si(Li) detector⁽¹⁾. Therefore, the efficiency calculations for the Si(Li) detector do not require corrections for escape peak losses. Experimental measurements^(1,5,6) of the escape peak losses for Ge(Li) detectors are in good agreement with both that predicted by the Axel model⁽⁵⁾ and with the Monte Carlo calculations⁽¹⁾.

Although the calculation of intrinsic detection efficiencies as outlined above predicts to first order the general features of the efficiency curves^(1,5), they are not reliable for determining absolute efficiencies. This, to a large extent, is a result of the differences in the real and nominal (as provided by the manufacturer) detector dimensions. However, the calculations are quite adequate for relative efficiencies provided one has a reasonable estimate of the real detector thickness.

One test of an efficiency curve derived from Equation (3) is to establish whether it will properly correct the measured relative K X-ray yields to the well known K β /K α transition probability ratios⁽⁷⁾ [cf. Section 1.1.4]. That is, the ratio of the efficiencies taken from a given efficiency curve for the K α and K β X-rays from element Z must be given by

$$\frac{\epsilon_{K\alpha}(Z)}{\epsilon_{K\beta}(Z)} = \frac{Y_{K\alpha}(Z)}{Y_{K\beta}(Z)} \frac{K\beta}{K\alpha}(Z) \frac{A_{K\beta}(Z)}{A_{K\alpha}(Z)} \frac{T_{K\beta}(Z)}{T_{K\alpha}(Z)}, \quad (5)$$

where $Y_{K\alpha}(Z)$ and $Y_{K\beta}(Z)$ are the measured relative yields for $K\alpha$ and $K\beta$ X-rays of element Z respectively (see Tables 3.2 and 3.3), $K\beta/K\alpha(Z)$ is the known transition probability ratio for element Z, and where the A and T terms are the absorption corrections for the X-rays as given in Section 3.2. If this relation holds over the entire range of elements, then the efficiency curve is adequate for obtaining relative efficiencies. Using the $Y_{K\alpha}(Z)$ and $Y_{K\beta}(Z)$ data from System D (see Table 3.3), the efficiency curve based on the nominal thickness of 3 mm for the Si(Li) detector miserably failed to satisfy the above test. For this reason, the nominal detector dimensions as reported by the manufacturer were considered unreliable and hence could not be used for the efficiency calculations. In contradistinction, the efficiency curve for the Ge(Li) detector derived using the nominal thickness of 4.8 mm, as reported by its manufacturer, did satisfy the relation of Equation (5) using the $Y_{K\alpha}(Z)$ and $Y_{K\beta}(Z)$ data from System C (see Table 3.2).

The relative intrinsic detection efficiency for the Ge(Li) detector over a large part of the X-ray region is rather invariant of the detector thickness. Below approximately 60 keV, ϵ_{photo} [Equation (1)] is inherently unity for any thickness in the range of several mm. As a result, the controlling factor in the efficiency, ϵ , as given by Equation (3), is the escape peak correction, R. By comparing experimentally determined values of R for a 4 mm thick detector⁽⁵⁾ to that for a 5 mm thick detector⁽⁶⁾, it is apparent that R is not very dependent on the thickness. Therefore, it should be suitable to utilize the

The absolute efficiency measurements were made in comparison to a standard 3" x 3" NaI(Tl) detector (Harshaw Integral Line Type 12S) using the NaI efficiency calculations of Heath⁽⁸⁾. For each efficiency value, measurements were made at several distances to eliminate systematic errors in locating the exact position of the sources. From a family of efficiency curves derived for a wide range of detector thicknesses, the curve which best fit the three absolute efficiencies was selected. The efficiency curve which resulted in the best fit was that derived with a detector thickness of 1.7 mm. The maximum uncertainty in the thickness was estimated to be \pm 0.2 mm. That is, the fitting procedure could definitely exclude any thickness greater than 1.9 mm or less than 1.5 mm.

The absolute efficiencies are dependent on the diameter of the detector crystal since their measurement requires an exact knowledge of the solid angle of the source subtended by the detector. For this reason, the absolute efficiency measurements cannot distinguish between a lower efficiency due to a reduced thickness or that due to a smaller diameter. Relative efficiency measurements obtained with sources containing at least two photons (X-rays or γ -rays) with known intensity ratios can make this distinction however, since they do not require a knowledge of the solid angle (viz. the detector diameter). For this procedure, the intensity ratios must be precisely known. Surprisingly, the ratio of Ag K X-rays to 88.1 keV γ -rays from ^{109}Cd is not as well known as one might suspect. This X/ γ intensity ratio has been reported as 26.0 ± 0.5 by Leutz, et. al.⁽⁹⁾ and Campbell, et. al.⁽⁶⁾, and as 22.6 ± 0.6 by Jensen and Wapstra⁽¹⁰⁾. There is no compelling reason to

have more confidence in either value over the other. The intensity ratio of 121.9 keV γ -rays to 14.36 keV γ -rays from ^{57}Co is better known. It has recently been reported as 8.99 ± 0.25 ⁽¹¹⁾. Using the above intensity ratios, the following relative efficiencies were obtained

$$\frac{I_{88}}{I_{K\alpha\beta}} = 26.0 \pm 0.5 \quad (6,9); \quad \frac{\epsilon_{88}}{\epsilon_{K\alpha}} = 0.025$$

$$\frac{I_{88}}{I_{K\alpha\beta}} = 22.6 \pm 0.6 \quad (10); \quad \frac{\epsilon_{88}}{\epsilon_{K\alpha}} = 0.021$$

$$\frac{I_{122}}{I_{14}} = 8.99 \pm 0.25 \quad (11); \quad \frac{\epsilon_{122}}{\epsilon_{14}} = 0.049$$

The efficiency curves which best fit these three relative efficiency values were those derived with thicknesses of 2.2 mm, 1.7 mm and 1.7 mm, respectively. Since both of the latter two values were in agreement with the thickness found from the absolute efficiency measurements, it appears that the nominal diameter of 4 mm for the detector is not in error.

In consideration of all of the above, the thickness of the Si(Li) detector was taken to be 1.7 ± 0.2 mm. Furthermore, the efficiency curve derived with this thickness adequately satisfied the relation of Equation (5) over the entire range of elements studied. Escape peak losses were neglected in the calculation since the magnitude of this effect was less than 1% for even the lowest energy X-ray measured with this detector. The relative efficiencies which were obtained from the curve for a 1.7 mm thick detector were tabulated in Table 3.8. The estimated error limits corresponding to a detector thickness

uncertainty of \pm 0.2 mm were also given in the Table.

- (1) H. I. Israel, D. W. Lier and E. Storm, Nucl. Instru. and Meth. 91, 141 (1971).
- (2) E. Storm and H. I. Israel, Nucl. Data A7, 565 (1970).
- (3) P. Axel, "Escape Peak Correction to Gamma Ray Intensity Measurements Made with Sodium-Iodide Crystals", Brookhaven National Laboratory, BNL Rpt. No. 271 (T-44), 1953.
- (4) W. Bambynek, B. Grasemann, R. W. Fink, H. U. Freund, Hans Mark, C. D. Swift, R. E. Price and P. Venugopala Rao, "X-Ray Fluorescence Yields and Coster-Kronig Transition Probabilities", unpublished compilation and review, 1972.
- (5) J. M. Palms, P. Venugopala Rao and R. E. Wood, Nucl. Instru. and Meth. 64, 310 (1968).
- (6) J. L. Campbell and L. A. McNelles, Nucl. Instru. and Meth. 98, 433 (1972).
- (7) G. C. Nelson, B. G. Saunders and S. I. Salem, Atomic Data 1, 377 (1970).
- (8) R. L. Heath, "Scintillation Spectrometry: Gamma-Ray Spectrum Catalog", Vol. 1, Second Edition, AEC Research and Development Rpt. IDO-16880-1, Physics, TID-4500, 1964.
- (9) H. Leutz, K. Schneckenberger and H. Wenninger, Nucl. Phys. 63, 263 (1966).
- (10) J. F. W. Jensen and A. H. Wapstra in "Internal Conversion Processes", J. H. Hamilton (Editor), Academic Press, N. Y., 1966, p. 237.
- (11) J. L. Campbell, P. O'Brien and L. A. McNelles, Nucl. Instru. and Meth. 92, 269 (1971).
- (12) A. Li-Scholz, W. Scholz, R. Collé and I. L. Preiss, to be published (1972).